Effect of Oxalate on Photodegradation of Bisphenol A at the Interface of Different Iron Oxides

ARTICLE *in* INDUSTRIAL & ENGINEERING CHEMISTRY RESEARCH · JANUARY 2007

Impact Factor: 2.59 · DOI: 10.1021/ie0612820

Effect of Oxalate on Photodegradation of Bisphenol A at the Interface of Different Iron Oxides

F. B. Li,[†,‡] X. Z. Li,[†,*] C. S. Liu,[‡] X. M. Li,[‡] and T. X. Liu[‡]

Department of Civil and Structural Engineering, The Hong Kong Polytechnic University, Hong Kong, China, and Guangdong Key Laboratory of Agricultural Environment Pollution Integrated Control, Guangdong Institute of Eco-Environment and Soil Science, Guangzhou 510650, China

In this study, a series of experiments were conducted to investigate the effect of the properties of iron oxides and oxalate on the degradation of bisphenol A (BPA) as a model organic pollutant in aqueous solution under UV illumination. Three iron oxides (Magh-300, Hem-420, and Hem-550) were prepared by a hydrothermal process and characterized by X-ray diffraction, the Brunauer−Emmett−Teller method, and scanning electron microscopy. The experimental results confirmed that the existence of oxalate can greatly enhance the BPA degradation reaction on the iron oxides in aqueous solution compared to iron oxides alone. The properties of iron oxides influenced strongly the dependence of the BPA degradation on the oxalate concentration. The optimal initial concentrations of oxalate were determined to be 2.4, 2.4, and 0.6 mM for Magh-300, Hem-420, and Hem-550, respectively. The optimal pH value was found to be 3.93, 3.64, and 3.61, for Magh-300, Hem-420, and Hem-550, respectively. The rate of BPA degradation on different iron oxides with oxalate under UV illumination can be ranked as Magh-300 > Hem-420 > Hem-550. Furthermore, it was found that the dependence of BPA degradation is also attributable to the interaction between iron oxide and oxalate, and the formation of dissolved Fe in the solution or adsorbed Fe−oxalate species on the surface of iron oxides.

Introduction

Many organic pollutants that are harmful to human beings exist in soil and water environments extensively.[1] However, these organic pollutants can be degraded on the surface of some minerals such as iron oxides under solar illumination in the natural environment.[2−4] Most iron oxides including maghemite (γ-Fe_2O_3), hematite (α-Fe_2O_3), lepidocrocite (γ-FeOOH), goethite (α-FeOOH), and magnetite (Fe_3O_4) have a narrow band gap (2.0−2.3 eV) and are photoactive under solar irradiation as photocatalysts or photosensitizers.[5,6]

Recently it was found that the degradation of organic pollutants in the natural environment can be accelerated by photo-Fenton-like reactions ($Fe^{3+}/H_2O_2/UV$) with iron oxides and polycarboxylic acids together.[7−9] These polycarboxylic acids with low-molecular-weights (LMW) are a kind of root exudates, released from plants.[10,11] Since this photo-Fenton-like oxidation process can utilize natural matters (iron oxides and LMW polycarboxylic acids) and solar energy for decontamination of organic pollutants in the environment, a better understanding of such photo-Fenton-like reactions becomes more attractive to scientists and also engineers. Among the LMW polycarboxylic acids, oxalic acid is one of the most active acids in the photo-Fenton-like reaction. In fact, the photochemistry of Fe(III)−oxalate complexes in aquatic environment, fog, precipitation, tropospheric aerosols, and soil solution has received considerable attention over the past three decades,[12−17] as Fe−oxalate exhibits strong ligand-to-metal charge absorption bands in the near-UV and visible region.

Up to now, a number of investigations have focused on the ferrioxalate/UV and ferrioxalate /H_2O_2/UV reactions for developing some engineered systems for wastewater treatment.[18−20] However, these systems should be categorized as homogeneous photochemical reactions with artificial addition of H_2O_2 chemical, but not the above-mentioned heterogeneous reactions occurring in the natural environment. In this study, bisphenol A (BPA)[21−24] was used as a model organic pollutant to study its degradation in an aqueous iron oxide−oxalate complex system under UV illumination affected by several key factors including the iron oxide properties, the oxalate concentrations, and pH in the range of 2.1−7.3.

Experimental Section

Preparation of Iron Oxides. Iron oxides (Fe_2O_3) were prepared with the following procedure:[25] 0.05 mol of hydrated ferric nitrate ($Fe(NO_3)_3{\cdot}9H_2O$) was dissolved in 80 mL of glycol and stirred strongly; then the solution was refluxed in a 250 mL flask at 70 °C for 24 h to obtain hydrosol; the hydrosol was then dried at 100 °C for 24 h to get xerogel. The xerogel was then ground and sintered at different high temperatures of 300, 420, and 550 °C for 2 h to obtain three different Fe_2O_3 powders named "Magh-300", "Hem-420", and "Hem-550", respectively.

Characterization of Iron Oxides. To determine the crystal phase composition of the prepared iron oxide samples, X-ray diffraction (XRD) measurement was carried out at room temperature using a Rigaku D/MAX-IIIA diffractometer with Cu Kα radiation (λ = 0.15418 nm). The accelerating voltage of 35 kV and emission current of 30 mA were used. Total surface area, micropore surface area, and total pore volume of all samples were measured by the Brunauer−Emmett−Teller (BET) method, in which the N_2 adsorption at 77 K was applied and a Carlo Erba Sorptometer was used. The surface morphology of the iron oxide samples was observed using scanning electron microscopy (SEM Leica Stereoscan 400i series).

Experimental Setup and Procedures. A Pyrex cylindrical photoreactor was used in the experiments to conduct photodegradation experiments, in which an 8 W LZC-UV lamp

* To whom correspondence should be addressed. Tel.: (852) 2766 6016. Fax: (852) 2334 6389. E-mail: cexzli@polyu.edu.hk.

[†] The Hong Kong Polytechnic University.

[‡] Guangdong Institute of Eco-Environment and Soil Science.

10.1021/ie0612820 CCC: $37.00
Published on Web 01/05/2007

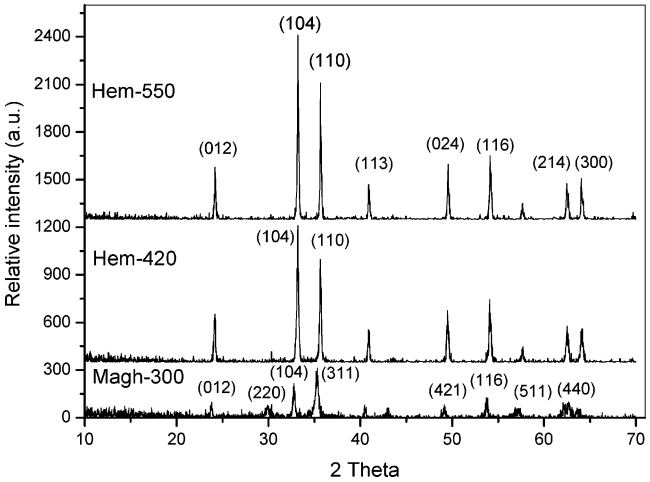

Figure 1. XRD graph of iron oxides powders.

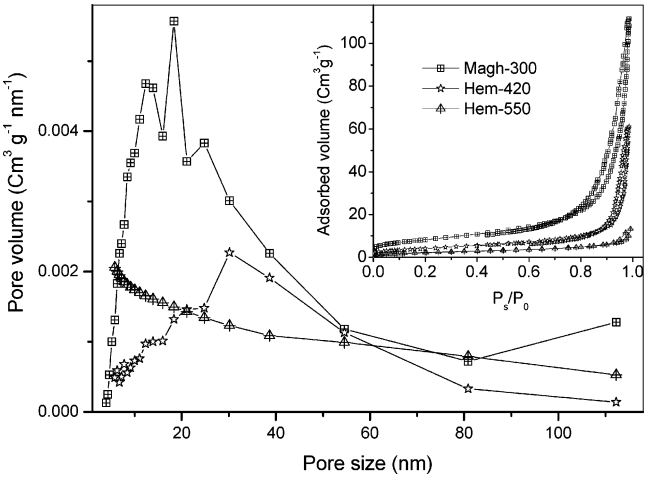

Figure 2. Pore size distribution of iron oxides. Insert: nitrogen adsorption−desorption isothermal curves of iron oxides.

(Luzchem Research, Inc.) with an emission peak at 365 nm is positioned at the center of the cylindrical vessel as a UV light source at the intensity of 1.20 mW cm^{-2}. This cylindrical photoreactor is surrounded by a Pyrex circulating water jacket to control the temperature during reaction and is covered by aluminum foil to avoid any indoor light irradiation. The reaction suspension was prepared by adding 0.25 g of iron oxides powder into 250 mL of aqueous BPA solution or the mixture solution of BPA and oxalic acid. Prior to the photoreaction, the suspension was magnetically stirred in the dark for 30 min to establish adsorption/desorption equilibrium between solid and solution. The aqueous suspension was irradiated by the UV light with constant aeration. At different time intervals, water samples were taken from the suspension, centrifuged for 20 min, and filtered through a 0.45 μm Millipore filter to remove the particles, and then stored in the dark before analysis.

Analytical Methods. The BPA concentration was determined by liquid chromatography (Finnigan LCQ DUO) with a UV detector. While a Pinnacle II C18 column (5 μm beads, 250 × 4.6 mm ID) was employed for BPA separation, a mobile phase of 70% HCN:30% water was pumped at a flow rate of 0.8 mL min^{-1}. The BPA concentration was determined by the UV detector at 278 nm. The oxalic acid concentration was determined by ion chromatography (Dionex DX-120), in which an ion column (IONPAC ASII-AC) together with a guard column (AGII-HC 4 mm) was used, and a mobile phase of 15 mM KOH solution was operated at a flow rate of 1.5 mL min^{-1}. Total adsorbed Fe ion and adsorbed Fe^{2+} were extracted by 0.1 mol L^{-1} HCl solution under 30 min of stirring. The concentration of total Fe ions was analyzed by atomic absorption spectrometry, while ferrous ion (Fe^{2+}) concentration was tested by the ferrozine method. The amount of H_2O_2 was tested at 528 nm using a H_2O_2 analyzer (ET-8600 Germany) with a detection limit of 0.03 mg L^{-1}.

Results and Discussion

Properties of Iron Oxides. Three iron oxides (Magh-300, Hem-420, and Hem-550) were examined by XRD and the analytical results are shown in Figure 1. The XRD pattern of Magh-300 showed five peaks (220), (311), (421), (511), and (440) attributable to maghemite and three peaks (012), (104), and (116) attributable to hematite, which means that Magh-300 had a mixed crystal structure of maghemite and hematite. The XRD patterns of Hem-420 and Hem-550 showed all peaks (012), (104), (110), (113), (024), (116), (214), and (300) attributable to hematite only. These results indicate that a phase transformation from maghemite to hematite was completed at a higher sintering temperature from 420 to 550 °C.

Table 1. Crystal Structure, Total Surface Area, Micropore Surface Area, and Total Pore Volume of Iron Oxides

parameter	Magh-300	Hem-420	Hem-550
crystal structure	maghemite/hematite	hematite	hematite
total surface area (m^2 g^{-1})	29.76	14.77	7.47
micropore surface area (m^2 g^{-1})	1.27	0.15	0
total pore volume (cm^3 g^{-1})	0.1558	0.0855	0.0059

The pore size distribution and nitrogen adsorption−desorption isothermal curves are shown in Figure 2. It can be seen clearly that the adsorbed nitrogen volume decreased significantly with the increased sintering temperature, and all isotherms are of Type IV curves.[23,24] The curves exhibit hysteresis loops at high relative pressures, indicating the presence of mesopores and macropores. The shape of the hysteresis loops are of Type H3. The distribution of hysteresis loops was at 0.7−0.98, 0.85−0.98, and 0.92−0.98 for Magh-300, Hem-420, and Hem-550, respectively. Magh-300 showed a mixed pore sizes of mesopores and macropores from 4 to 112 nm with three peaks at 12.33, 18.36, and 24.8 nm. Hem-420 showed mixed pore sizes of mesopores and macropores from 5.8 to 112 nm with a peak at 30.17 nm. Hem-550 also showed a mixed pore sizes of mesopores and macropores in the similar range. Total surface area, micropore surface area, and total pore volume of iron oxides were determined by the BET method, and the results are listed in Table 1. Total surface areas of Magh-300, Hem-420, and Hem-550 were determined to be 29.76, 14.77, and 7.47 m^2 g^{-1}, respectively, and their total pore volumes to be 0.1558, 0.0855, and 0.0059 cm^3 g^{-1}. These BET data indicate that total surface area decreased with the increased temperature because the larger particle size and pore sizes were formed at higher sintering temperature as shown in Figure 3. Among them, Magh-300 had the largest total surface area, micropore surface area, and total pore volume, while Hem-550 had the smallest values.

The morphology of iron oxides was examined by SEM, and three images of Magh-300, Hem-420, and Hem-550 are shown in Figure 3. These images showed different structures. Magh-300 has a spongy leaves-like structure and Hem-420 has a nodule-like structure, while Hem-550 has a coral-like structure owing to the growth and aggregation of iron oxide particles. It

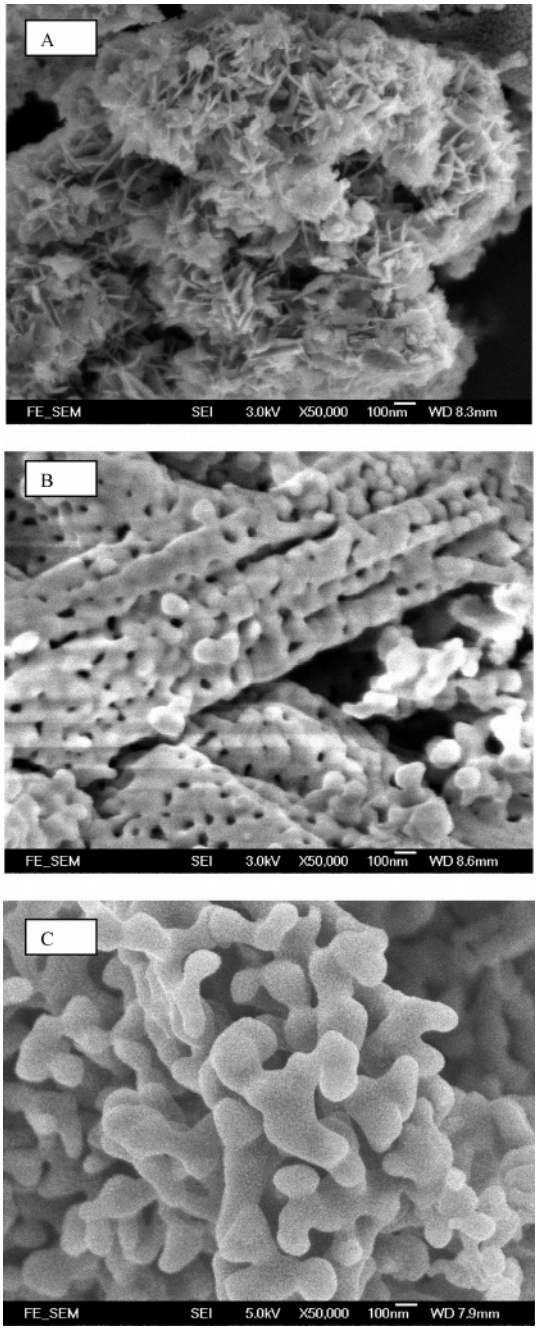

Figure 3. SEM photograph of Magh-300 (A), Hem-420 (B), and Hem-550 (C).

can be seen that all samples have porous structures,[26,27] but with different pore sizes. While Hem-420 has mainly mesopores in a size range of 20−60 nm, Hem-550 has many macropores in a bigger size of around 100 nm.

Photodegradation of BPA under Different Conditions. Figure 4 showed BPA degradation in aqueous suspension with an initial concentration (C_{BPA}) of 0.103 mM under different reaction conditions. The BPA removal percentage and the first-order kinetic constants (k) are listed in Table 2. Obviously, the BPA removal after 60 min was only achieved by 2.1% in the dark due to adsorption on the surface of iron oxide alone (curve a) and by 3.3% only under UV illumination (curve b); while that was achieved by 23.8% in the Hem-420 suspension without oxalic acid under UV illumination (curve c). The BPA removals and k values were greatly enhanced with iron oxides and oxalic acids together (curves d, e, and f). The k values are ranked in an order of Magh-300 > Hem-420 > Hem-550. These results

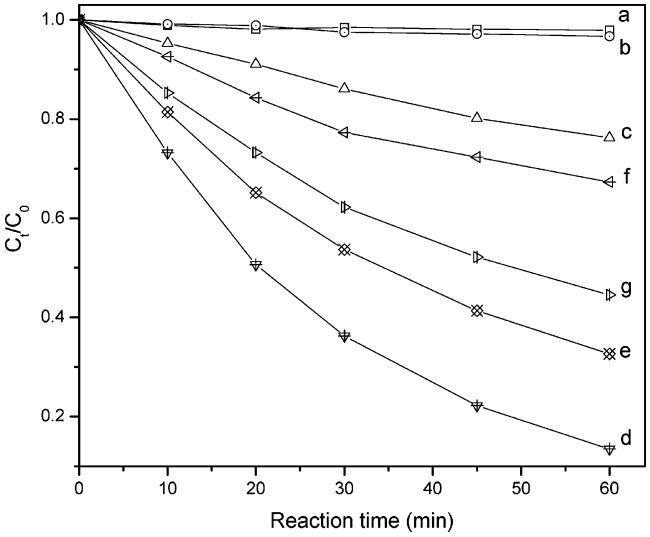

Figure 4. Photodegradation of 0.103 mM BPA under different conditions: (a) 1.2 mM oxalic acid + 1.0 g L^{-1} Hem-420, (b) UV, (c) UV + 1.2 g L^{-1} Hem-420, (d) 1.0 g L^{-1} Magh-300 + UV + 1.2 mM oxalic acid, (e) 1.0 g L^{-1} Hem-420 + UV + 1.2 mM oxalic acid, (f) 1.0 g L^{-1} Hem-550 + UV + 1.2 mM oxalic acid, (g) 86 mg L^{-1} Fe^{3+} + UV + 1.2 mM oxalic acid.

Table 2. Summary of Experimental Data under Different Reaction Conditions in Figure 4

reaction conditions	removal (%)	k (min^{-1})	R^2
a	2.1	−	−
b	3.3	−	−
c	23.8	$(0.47 \pm 0.016) \times 10^{-2}$	0.995
d	86.5	$(3.55 \pm 0.026) \times 10^{-2}$	0.999
e	67.4	$(1.94 \pm 0.061) \times 10^{-2}$	0.996
f	32.7	$(0.72 \pm 0.052) \times 10^{-2}$	0.975
g	55.4	$(1.36 \pm 0.062) \times 10^{-2}$	0.992

showed that iron oxides, oxalate, and UV light are three essential factors in the BPA degradation. In addition, the properties of iron oxides and the cooperation of iron oxide and oxalate during the reaction also play important roles in the BPA degradation. The photochemical process in the presence of iron oxide and oxalate together has been described in detail by some researchers.[7,8,17] In such an aqueous suspension, a series of reactions could be described by reactions 1−9. Generally, oxalic acid is first adsorbed on the surface of iron oxide to form iron oxide−oxalate complexes of $[\equiv Fe^{III}(C_2O_4)_n]^{3-2n}$ (reaction 1), which can be excited to form a series of radicals including oxalate radical $(C_2O_4)^{\bullet -}$, carbon-centered radical $(CO_2)^{\bullet -}$, superoxide ion $(O_2^{\bullet -})$, $^{\bullet}OOH$ and hydroxyl radical ($^{\bullet}OH$), and then to form H_2O_2 (reactions 2−9). The dissolved $[Fe^{III}(C_2O_4)_n]^{3-2n}$ in the solution can be formed. In our experiments, the H_2O_2 concentration during the photoreaction was detected at a level below 0.50 mg L^{-1}. It must be noted that this photochemical process happened both on the surface of iron oxide as a heterogeneous reaction and also in the solution as a homogeneous reaction. To compare the efficiency in iron oxide−oxalate heterogeneous system with that in Fe(III)−oxalate homogeneous system, a homogeneous system was set up by adding 0.6 mM Fe^{3+} (same concentration in Hem-420 and oxalate suspension) and 1.2 mM oxalate to degrade BPA under 1.2 mW cm^{-2} UV irradiation, as shown in curve g in Figure 4. The results showed that the BPA removal was only 55.4%, much lower than that in the heterogeneous system, when the same light intensity was applied in the both reaction systems. This result may indicate that the BPA degradation in iron oxide−oxalate suspension was achieved at a higher efficiency than that in the homogeneous system.

$$\text{iron oxide} + n\text{H}_2\text{C}_2\text{O}_4 \leftrightarrow [\equiv\text{Fe}(\text{C}_2\text{O}_4)_n]^{(2n-3)-} \quad (1)$$

$$[\equiv\text{Fe}(\text{C}_2\text{O}_4)_n]^{(2n-3)-} + h\nu \rightarrow \text{Fe}(\text{C}_2\text{O}_4)_2^{2-} \text{ (or } \equiv\text{Fe}(\text{C}_2\text{O}_4)_2^{2-}) + (\text{C}_2\text{O}_4)^{\bullet-} \quad (2)$$

$$\text{Fe}^{\text{III}}(\text{C}_2\text{O}_4)_n^{3-2n} + h\nu \rightarrow [\text{Fe}^{\text{II}}(\text{C}_2\text{O}_4)_{(n-1)}]^{4-2n} + (\text{C}_2\text{O}_4)^{\bullet-} \quad (3)$$

$$(\text{C}_2\text{O}_4)^{\bullet-} \rightarrow \text{CO}_2 + \text{CO}_2^{\bullet-} \quad (4)$$

$$\text{CO}_2^{\bullet-} + \text{O}_2 \rightarrow \text{CO}_2 + \text{O}_2^{\bullet-} \quad (5)$$

$$\text{O}_2^{\bullet-} + \text{H}^+ \rightarrow {}^{\bullet}\text{OOH} \quad (6)$$

$$\text{O}_2^{\bullet-} + \text{Fe}^{3+} \rightarrow \text{Fe}^{2+} + \text{O}_2 \quad (7)$$

$$\text{O}_2^{\bullet-}/{}^{\bullet}\text{OOH} + n\text{H}^+ + \text{Fe}^{2+} \rightarrow \text{Fe}^{3+} + \text{H}_2\text{O}_2 \quad (8)$$

$$\text{Fe}^{2+} + \text{H}_2\text{O}_2 \rightarrow \text{Fe}^{3+} + \text{OH}^- + {}^{\bullet}\text{OH} \quad (9)$$

Effect of Oxalate on BPA Photodegradation. The photodegradation of BPA in aqueous solution with iron oxide and oxalic acid together as the photo-Fenton-like reaction is actually complicated, in which oxalate plays a critical role through the reactions 1−9. To study the effect of oxalate on the photodegradation of BPA, three sets of experiments with $C_{BPA} = 0.157$, 0.103, and 0.0821 mM for Magh-300, Hem-420, and Hem-550, respectively, with a common iron oxide load of 1 g L^{-1} were conducted under UV illumination, in which each set of experiments was performed with different initial concentrations of oxalic acid (C_{ox}) in the range of 0.4−3.6 mM. The experimental results are shown in Figure 5A−C. It is very obvious that the presence of oxalate could greatly enhance the BPA photodegradation in aqueous iron oxide suspensions. The results showed that the BPA degradation was significantly increased with the increase of oxalate concentration in its low range, but it was slightly inhibited with an excessive amount of oxalate. The experimental data of BPA degradation were well fitted by using the first-order kinetic model and the first-order kinetic constants (k) with different C_{ox} were determined and are listed in Table 3. It can be seen that the k values of all catalysts are affected by the oxalate concentration significantly for all three catalysts. These results indicate there is an optimal C_{ox} to achieve the best performance of BPA degradation. Under this experimental condition, three optimal C_{ox} values to achieve the best performance of BPA degradation under UV illumination were found to be 2.4, 2.4, and 0.6 mM for Magh-300, Hem-420, and Hem-550, respectively. Balmer and Sulzberger[17] reported that Fe^{3+} mainly presented as $Fe(C_2O_4)_2^-$ and $Fe(C_2O_4)_3^{3-}$ in the Fe^{3+}−oxalate system when the concentration of oxalate was more than 0.18 mM. $Fe(C_2O_4)_2^-$ and $Fe(C_2O_4)_3^{3-}$ are much more efficiently photolyzed than other Fe^{3+} speciation. In our experiments, the higher concentration of oxalate could result in higher concentrations of $Fe^{III}(C_2O_4)_2^-$ and $Fe^{III}(C_2O_4)_3^{3-}$ in the solution and also those of $[\equiv Fe^{III}(C_2O_4)_2]^-$ and $[\equiv Fe^{III}(C_2O_4)_3]^{3-}$ on the surface of iron oxides, and eventually forms more radicals to lead to a higher degree of BPA degradation. However, excessive oxalate would occupy the adsorbed sites on the surface of iron oxide and also reacts competitively with hydroxyl radicals, which results in less hydroxyl radicals available for BPA degradation. Furthermore, excessive oxalate would lead to the formation of a large amount of Fe^{3+}, which would inhibit the formation of H_2O_2. Therefore, there should be an optimal concentration of oxalate for the BPA photodegradation reaction.

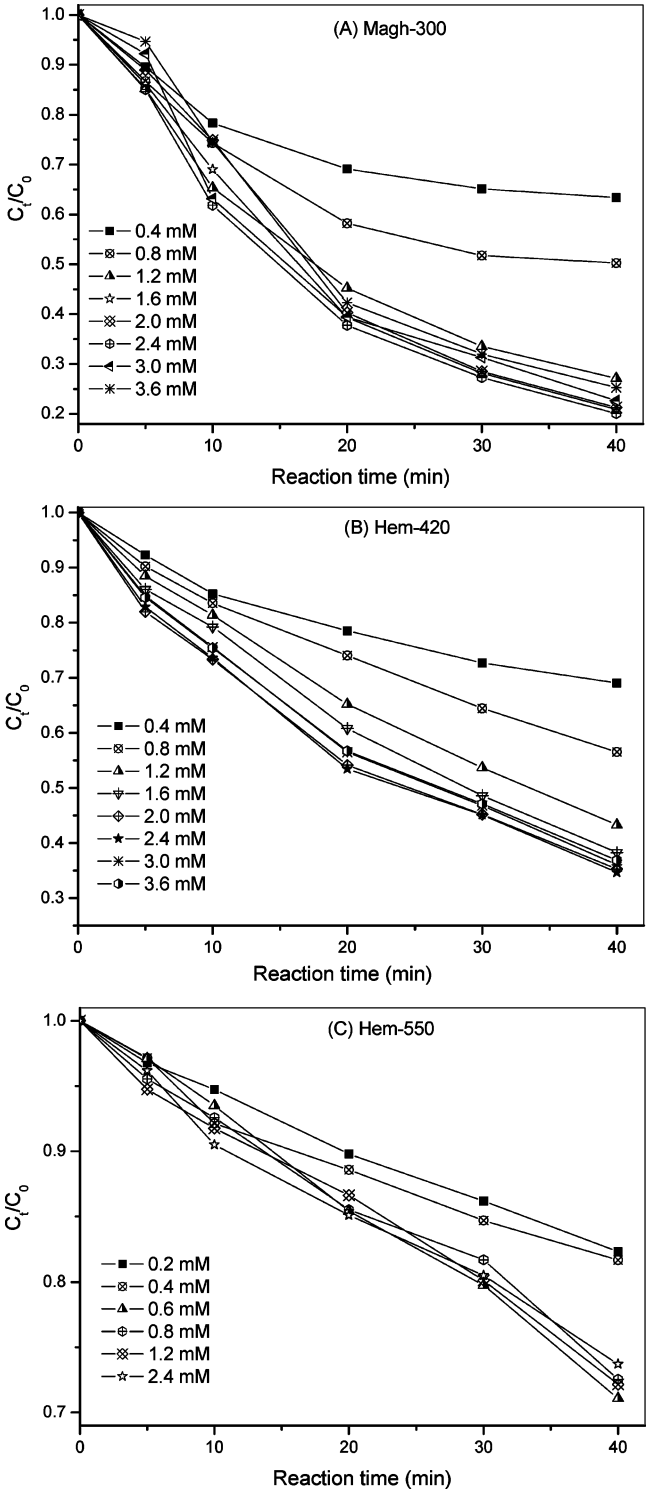

Figure 5. Effect of the initial concentration of oxalic acid (C_{ox}) on BPA degradation under UV illumination on Magh-300 with $C_{BPA} = 0.157$ mM (A), Hem-420 with $C_{BPA} = 0.103$ mM (B), and Hem-550 with $C_{BPA} = 0.0821$ mM (C).

Effect of pH Value on BPA Photodegradation. To investigate the effect of pH value on BPA photodegradation, a set of experiments was carried out with 1.0 g L^{-1} iron oxides in the presence of BPA ($C_{BPA} = 0.103$ mM) and oxalate ($C_{ox} = 1.2$ mM) under UV light irradiation. The pH value was adjusted by adding NaOH or $HClO_4$ before the reaction. The dependence of the first-order kinetic constant k values on pH value is presented in Figure 6. The results showed that BPA photodeg-

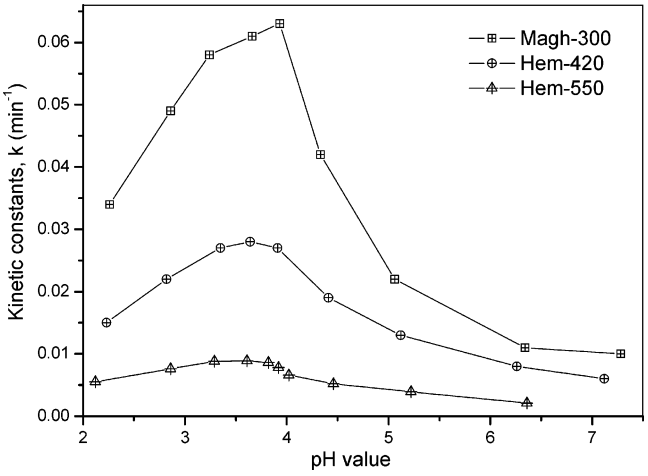

Figure 6. Dependence of the first-order kinetic constant k value on the pH value in the solution by using 1.0 g L^{-1} iron oxides in the presence of BPA with the initial concentration of 0.103 mM and oxalate with the initial concentration of 1.2 mM under UVA light.

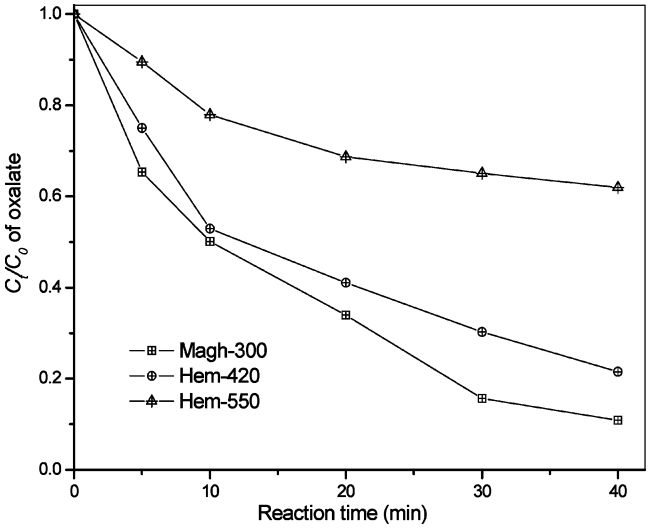

Figure 7. Photodegradation of oxalate with $C_{ox} = 2.4$ mM in presence of BPA under UV illumination with $C_{BPA} = 0.103$ mM in the aqueous iron oxide suspension.

radation should depend strongly on the pH value in the iron oxide−oxalate system. The BPA degradation would be inhibited significantly when pH values were beyond the range of about 3−4. Obviously, there was an optimal pH value for BPA degradation. The optimal pH value might be at 3.93, 3.64, and 3.61, for Magh-300, Hem-420, and Hem-550, respectively. It can be concluded that the pH value should be a very important factor affecting this photo-Fenton-like reaction.

Balmer and Sulzberger[17] had reported that when the pH was at around 4 in homogeneous Fe(III)−oxalate system, the main Fe^{III} species were $Fe^{III}(C_2O_4)_2^-$ and $Fe^{III}(C_2O_4)_3^{3-}$, which are highly photoactive. And in our experiment, the iron oxide−oxalate complex system at pH value of about 3−4 might have a higher concentration of $Fe^{III}(C_2O_4)_2^-$ and $Fe^{III}(C_2O_4)_3^{3-}$ in the solution, and $[\equiv Fe^{III}(C_2O_4)_2]^-$ and $[\equiv Fe^{III}(C_2O_4)_3]^{3-}$ on the surface. However, the optimal pH value should depend on the properties of iron oxides in this heterogeneous system. As the mentioned above, Hem-420 and Hem-550 with pure α-Fe_2O_3 phase had the more stable thermodynamics and lower specific surface area than Magh-300 with a mixed phase of γ-Fe_2O_3 and α-Fe_2O_3.[8] It is difficult for Hem-420 and Hem-550 to form ≡Fe(III)−oxalate complexes on their surfaces, and then the concentration of dissolved iron in the solution is at a low level. But lower pH can enhance the dissolution of iron oxides and the formation of Fe(III)−oxalate complexes in the solution and ≡Fe(III)−oxalate complexes on the surface, which might lead to the lower optimal pH value. However, any excessive decrease of pH value will lead to the formation of excessive Fe^{3+} and the dissolution of iron oxides, which should be not beneficial to this photo-Fenton-like reaction. When the pH value increased to about 4−5, Fe(^{III})−oxalate species were mainly $Fe^{III}(C_2O_4)^+$ and $[\equiv Fe^{III}(C_2O_4)]^+$, which are low photoactive. When the pH value was up to 6, the Fe^{3+} and Fe^{2+} almost cannot exist in the solution and the predominant Fe(III) and Fe(II) species were Fe(II)-OH and Fe(III)-OH as the precipitate, which might hardly be photoactive.

Photodegradation of Oxalate and Variation of pH Value. Once the BPA degradation on iron oxide under UV illumination can be enhanced by oxalate as a main reaction, the oxalate itself is also degraded simultaneously as a side reaction. In the meantime, pH increases along with the degradation of oxalate during photoreaction. To better understand this reaction, the variations of oxalate concentration and pH during the BPA degradation reaction were investigated in a set of experiments under UV illumination. Three reaction suspensions ($C_{ox} = 2.4$ mM and $C_{BPA} = 0.103$ mM) containing different catalysts (Magh-300, Hem-420, and Hem-550) were irradiated by UV light for 40 min, respectively. The experimental results are summarized in Figure 7. All experimental data were well fitted by the first-order kinetic model. The first-order kinetic constants (k) of oxalate reduction reaction for Magh-300, Hem-420, and Hem-550 were found to be $(5.79 \pm 0.31) \times 10^{-2}$, $(4.06 \pm 0.29) \times 10^{-2}$, and $(1.41 \pm 0.19) \times 10^{-2}$ min^{-1} under UV illumination, respectively. The experimental results showed that the reduction of oxalate strongly depended on the iron oxides. Magh-300 had the highest activity for oxalate reduction ranked as Magh-300 > Hem-420 > Hem-550 under UV illuminations. The results indicate that Magh-300 achieved best performance in both the BPA degradation and oxalate degradation. Due to its high specific surface area and the less thermodynamical stability,

Table 3. Dependence of the Apparent First-Order Kinetic Constant (k) on the Initial Concentration of Oxalic Acid (C_{ox})

	Magh-300		Hem-420			Hem-550	
C_{ox} (mM)	k (min^{-1})	R^2	k (min^{-1})	R^2	C_{ox} (mM)	k (min^{-1})	R^2
0	0.0018 ± 0.0002	0.960	0.0034 ± 0.0009	0.991	0	0.0021 ± 0.0001	0.998
0.4	0.0198 ± 0.002	0.961	0.0103 ± 0.0005	0.930	0.2	0.0050 ± 0.0004	0.994
0.8	0.0240 ± 0.002	0.962	0.0147 ± 0.0003	0.990	0.4	0.0054 ± 0.0004	0.963
1.2	0.0350 ± 0.002	0.981	0.0210 ± 0.0004	0.999	0.6	0.0081 ± 0.0005	0.989
1.6	0.0409 ± 0.003	0.988	0.0242 ± 0.001	0.998	0.8	0.0076 ± 0.0004	0.985
2.0	0.0401 ± 0.002	0.982	0.0271 ± 0.001	0.983	1.2	0.0078 ± 0.0004	0.989
2.4	0.0424 ± 0.003	0.985	0.0274 ± 0.0008	0.986	2.4	0.0076 ± 0.0004	0.988
3.0	0.0389 ± 0.003	0.987	0.0260 ± 0.0009	0.993			
3.6	0.0362 ± 0.002	0.972	0.0256 ± 0.0008	0.991			

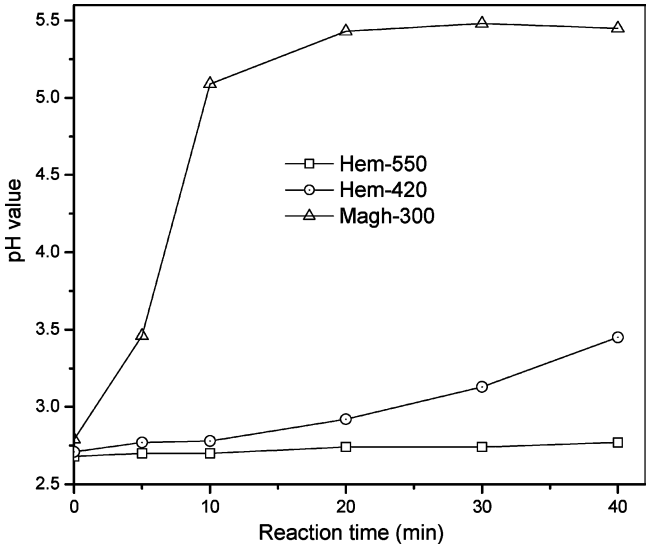

Figure 8. pH value in the solution plots on the reaction time with C_{ox} = 2.4 mM in presence of BPA under UV illumination with C_{BPA} = 0.103 mM in the iron oxide suspension.

Magh-300 can complex with oxalate more easily than Hem-420 and Hem-550.[8,28]

At the meantime, the pH value was simultaneously determined under the same conditions. The variations of pH vs reaction time are plotted in Figure 8. The results showed that the pH increased significantly from 2.79, 2.71, and 2.68 to 5.45, 3.45, and 2.77 after 40 min for Magh-300, Hem-420, Hem-550, respectively, under UV light irradiation. The higher initial pH value in the iron oxide suspension should be attributable to the stronger adsorption of oxalate on the surface of iron oxides. The results showed that the initial pH values were ranked as Magh-300 > Hem-420 > Hem-550. These results indicate that Magh-300 with a higher specific surface area and active thermodynamics can more easily adsorb and complex with oxalate and then led to a higher initial pH value in the solution. During the photochemical process, $^{\bullet}OH$ is generated in accompaniment with the generation of OH^- by reaction 9, and the formation of $^{\bullet}OOH$ and hydroxyl radical ($^{\bullet}OH$) need to consume H^+ by the reactions 6 and 8. Therefore, while more $^{\bullet}OOH$ and $^{\bullet}OH$ radicals are formed, more H^+ will be in the solution, and the degree of pH increase can be ranked as Magh-300 > Hem-420 > Hem-550.

Formation of Fe−Oxalate Species. During the reactions of BPA and oxalate degradations, some complexes of $[\equiv Fe^{III}(C_2O_4)_n]^{3-2n}$ and $[\equiv Fe^{II}(C_2O_4)_n]^{2-2n}$ are initially formed on the surface of iron oxide after adsorption of oxalate from solution, then can be dissolved under UV illumination, and form $[Fe^{III}(C_2O_4)_n]^{3-2n}$ and $[Fe^{II}(C_2O_4)_n]^{2-2n}$ in the solution. To study the formation of Fe−oxalate species, the experiments using different catalysts (Magh-300, Hem-420, and Hem-550) were conducted under UV illumination with C_{ox} = 1.2 mM and C_{BPA} = 0.103 mM, in which dissolved Fe^{3+} and Fe^{2+} species were monitored during the BPA degradation reaction, as shown in Figure 9. Figure 9A showed that the concentration of dissolved Fe^{3+} species in the solution was the highest at the beginning of photoreaction and then decreased gradually along with reaction time under UV illumination. However, the concentration of dissolved Fe^{2+} species on the surface of iron oxide increased quickly during the first 10 min and then decreased gradually along with reaction time for Magh-300, while it increased during the first 30 min and then decreased for Hem-420, and increased slowly all the time for Hem-550 under UV illumination. The dissolved Fe^{2+} species formed by the reduction of the dissolved Fe^{3+} species. Figure 9B showed that the concentration of adsorbed Fe^{2+} should be much more than that of adsorbed Fe^{3+}, and the concentration of adsorbed Fe^{2+} remained at a higher level for Magh-300 and Hem-420.

Importantly, the formation of Fe−oxalate species depends on the crystal structure of iron oxides. The experimental results in this study demonstrated that the dissolved or adsorbed Fe−oxalate species was most easily formed in Magh-300 suspension, while it was much more slowly formed in Hem-550 suspension under UV illumination. Hem-550 with pure α-Fe_2O_3 phase has more stable thermodynamics and much lower specific surface area than Magh-320, which has the mixed phase of γ-Fe_2O_3 and α-Fe_2O_3 and a higher specific surface area. It is difficult to form ≡Fe(III)−oxalate complexes on the surface of Hem-550, and then the concentration of dissolved iron in the solution was at a low level. The smaller amount of ≡Fe(III)−oxalate complexes on the surface of Hem-550 led to lower photochemical activity. The formation of Fe−oxalate species under UV

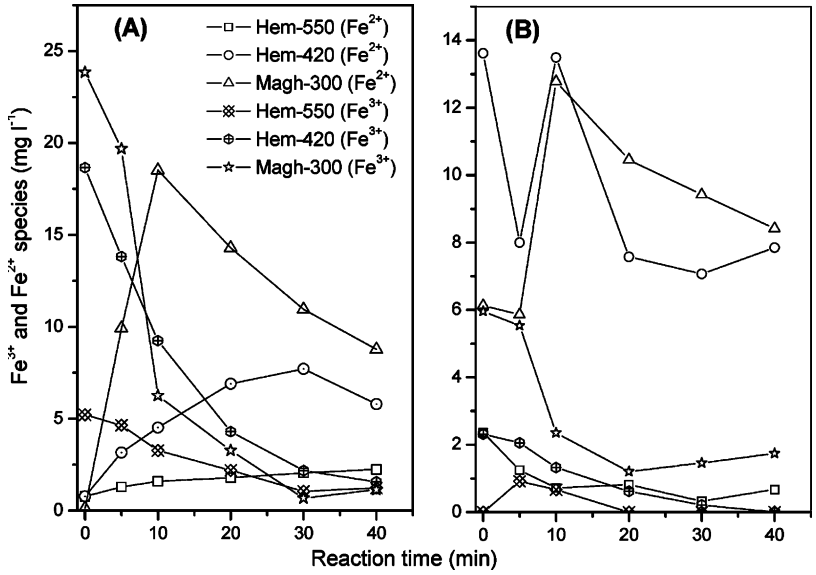

Figure 9. Concentration of dissolved Fe^{3+} and Fe^{2+} species in the solution (A) and adsorbed Fe^{3+} and Fe^{2+} species on the surface (B) plots on reaction time with C_{ox} = 1.2 mM in presence of BPA with C_{BPA} = 0.103 mM under UV illumination.

illuminations can be ranked as Magh-300 > Hem-420 > Hem-550, following the order of k values for BPA degradation.

Conclusions

The experimental results confirmed clearly that (1) BPA degradation can be affected by the properties of iron oxides ranked as Magh-300 > Hem-420 > Hem-550 and (2) the existence of oxalate together with iron oxides can enhance degradation of BPA in aqueous solution with a much faster rate than iron oxides alone. The optimal C_{ox} for BPA degradation was determined to be 2.4, 2.4, and 0.6 mM under UV illumination for Magh-300, Hem-420, and Hem-550, respectively. The optimal pH value was found to be 3.93, 3.64, and 3.61, for Magh-300, Hem-420, and Hem-550, respectively. The difference of BPA degradation among different iron oxides should be attributable to the difference of the interaction between iron oxides and oxalate and to the formation of Fe−oxalate species.

Acknowledgment

The authors thank the Hong Kong Government Research Grant Committee for financial support to this work under the RGC Grant (PolyU 5170/04E) and China National Natural Science Foundation (No. 20377011) and Guangdong Natural Science Foundation Key Project (No. 036533).

Literature Cited

(1) Valle, M. D.; Jurado, E.; Dachs, J.; Sweetman, A. J.; Jones, K. C. The maximum reservoir capacity of soils for persistent organic pollutants: implications for global cycling. *Environ. Pollut.* **2005**, *134*, 153−164.

(2) Schoonen, M. A. A.; Xu, Y.; Strongin, D. R. An introduction to geocatalysis. *J. Geochem. Explor.* **1998**, *62*, 201−215.

(3) Swearingen, C.; Macha, S.; Fitch, A. Leashed ferrocenes at clay surfaces: potential applications for environmental catalysis. *J. Mol. Catal. A: Chem.* **2003**, *199*, 149−160.

(4) Rhoton, F. E.; Bigham, J. M.; Lindbo, D. L. Properties of iron oxides in streams draining the Loess Uplands of Mississippi. *Appl. Geochem.* **2002**, *17*, 409−419.

(5) Schwertmann, U.; Cornell, R. M. *Iron oxides in the laboratory: preparation and characterization*, 2nd ed.; WILEY-VCH: New York, 2000.

(6) Leland, J. K.; Bard, A. J. Photochemistry of colloidal semiconducting iron oxide polymorphs. *J. Phys. Chem.* **1987**, *91*, 5076−5083.

(7) Zuo, Y. G. Deng, Y. W. Iron(II)-catalyzed photochemical decomposition of oxalic acid and generation of H_2O_2 in atmospheric liquid phases. *Chemosphere* **1997**, *35*, 2051.

(8) Siffert, C.; Sulzberger, B. Light-induced dissolution of hematite in the presence of oxalate. A case study. *Langmuir* **1991**, *7*, 1627−1634.

(9) Faust, B. C.; Zepp, R. G. Photochemistry of aqueous iron(III)-polycarboxylate complexes: roles in the chemistry of atmospheric and surface waters. *Environ. Sci. Technol.* **1993**, *27*, 2517−2522.

(10) Strobel, B. W. Influence of vegetation on low-molecular-weight carboxylic acids in soil solution—a review. *Geoderma* **2001**, *99*, 169−198.

(11) Ma, J. F.; Zheng, S. J.; Matsumoto, H.; Hiradate, S. Detoxifying aluminum with buckwheat. *Nature* **1997**, *390*, 569−570.

(12) Bozzi, A.; Yuranova, T.; Mielczarski, J.; Lopez, A.; Kiwi, J. Abatement of oxalates catalyzed by Fe-silica structured surfaces via cyclic carboxylate intermediates in photo-Fenton reactions. *Chem. Commu.* **2002**, *8*, 2202−2203.

(13) Zepp, R. G.; Faust, B. C.; Hoigne, J. Hydroxyl radical formation in aqueous reactions (pH 3−8) of iron(II) with hydrogen peroxide: the photo-Fenton reaction. *Environ. Sci. Technol.* **1992**, *26*, 313−319.

(14) P. Mazellier, B. Sulzberger, Diuron Degradation in Irradiated, Heterogeneous Iron/Oxalate Systems: The Rate-Determining Step. *Environ. Sci. Technol.* **2001**, *35*, 3314−3320.

(15) Nadtochenko, V.; Kiwi, J. Photoinduced adduct formation between Orange II and $[Fe^{3+}(aq)]$ or $Fe(ox)_3^{3-}$−H_2O_2 Photocatalytic degradation and laser spectroscopy. *J. Chem. Soc., Faraday Trans.* **1997**, *93*, 2373−2378.

(16) Zuo, Y. G.; Holgné, J. Formation of hydrogen peroxide and depletion of oxalic acid in atmospheric water by photolysis of iron(III)-oxalato complexes. *Environ. Sci. Technol.* **1992**, *26*, 1014−1022.

(17) Balmer, M. E.; Sulzberger, B. Atrazine Degradation in Irradiated Iron/Oxalate Systems: Effects of pH and Oxalate. *Environ. Sci. Technol.* **1999**, *33*, 2418−2424.

(18) Huston, P.; Pignatello, J. J. Reduction of Perchloroalkanes by Ferrioxalate-Generated Carboxylate Radical Preceding Mineralization by the Photo-Fenton Reaction. *Environ. Sci. Technol.* **1996**, *30*, 3457−3463.

(19) Jeong, J.; Yoon, J. Dual roles of $CO_2^{-\bullet}$ for degrading synthetic organic chemicals in the photo/ferrioxalate system. *Wat. Res.* **2004**, *38*, 3531−3540.

(20) Lee, Y.; Jeong, J.; Lee, C.; Kim, S.; Yoon, J. Influence of various reaction parameters on 2,4-D removal in photo/ferrioxalate/H_2O_2 process. *Chemosphere* **2003**, *51*, 901−912.

(21) Cousins, I. T.; Staples, C. A.; Klecka, G. M.; Mackay, D. A Multimedia Assessment of the Environmental Fate of Bisphenol A. *Hum. Ecol. Risk Assess.* **2002**, *8*, 1107−1135.

(22) Fukahori, S.; Ichiura, H.; Kitaoka, T.; Tanaka, H. Photocatalytic Decomposition of Bisphenol A in Water Using Composite TiO_2-Zeolite Sheets Prepared by a Papermaking Technique. *Environ. Sci. Technol.* **2003**, *37*, 1048−1051.

(23) Fukahori, S.; Ichiura, H.; Kitaoka, T.; Tanaka, H. Capturing of bisphenol A photodecomposition intermediates by composite TiO_2−zeolite sheets. *Appl. Catal. B: Environ.* **2003**, *46*, 453−462.

(24) Ooka, C.; Yoshida, H.; Horio, M.; Suzuki, K.; Hattori, T. Adsorptive and photocatalytic performance of TiO_2 pillared montmorillonite in degradation of endocrine disruptors having different hydrophobicity. *Appl. Catal. B: Environ.* **2003**, *41*, 313−321.

(25) Tao, S.; Liu, X.; Chu, X.; Shen, Y. Preparation and properties of γ-Fe_2O_3 and Y_2O_3 doped γ-Fe_2O_3 by a sol−gel process. *Sens. Actuator B: Chem.* **1999**, *61*, 33−38.

(26) Yu, J. G.; Yu, J. C.; Leung, M. K. P.; Ho, W.; Cheng, K. B.; Zhao, X. J.; Zhao, J. C. Effects of acidic and basic hydrolysis catalysts on the photocatalytic activity and microstructures of bimodal mesoporous titania. *J. Catal.* **2003**, *217*, 69−78.

(27) Yu, J. G.; Yu, J. C.; Cheng, B.; Hark, S. K.; Iu, K. The effect of F^--doping and temperature on the structural and textural evolution of mesoporous TiO_2 powders. *J. Solid State Chem.* **2003**, *174*, 372−380.

(28) Liu, C. S.; Li, F. B.; Li, X. M.; Zhang, G.; Kuang, Y. Q. The effect of iron oxides and oxalate on the photodegradation of 2-mercaptobenzothiazole. *J. Mol. Catal. A: Chem.* **2006**, *252*, 40−48.

Received for review October 6, 2006
Revised manuscript received November 19, 2006
Accepted November 22, 2006

IE0612820